applied sciences

MDPI

Article

Plasmonics in the Ultraviolet with Aluminum, Gallium, Magnesium and Rhodium

Yael Gutiérrez, Rodrigo Alcaraz de la Osa, Dolores Ortiz, José María Saiz, Francisco González and Fernando Moreno *

Department of Applied Physics, University of Cantabria, Avda. Los Castros, s/n, 39005 Santander, Spain; gvelay@unican.es (Y.G.); alcarazr@unican.es (R.A.d.l.O.); ortizd@unican.es (D.O.); saizvj@unican.es (J.M.S.); gonzaleff@unican.es (F.G.)

* Correspondence: morenof@unican.es

Received: 5 December 2017; Accepted: 28 December 2017; Published: 4 January 2018

Abstract: Ultraviolet plasmonics (UV) has become an active topic of research due to the new challenges arising in fields such as biosensing, chemistry or spectroscopy. Recent studies have pointed out aluminum, gallium, magnesium and rhodium as promising candidates for plasmonics in the UV range. Aluminum and magnesium present a high oxidation tendency that has a critical effect in their plasmonic performance. Nevertheless, gallium and rhodium have drawn a lot of attention because of their low tendency of oxidation and, at the same time, good plasmonic response in the UV and excellent photocatalytic properties. Here, we present a short overview of the current state of UV plasmonics with the latest findings in the plasmonic response and applications of aluminum, gallium, magnesium and rhodium nanoparticles.

Keywords: ultraviolet; plasmonics; UV plasmonics; aluminum; gallium; magnesium; rhodium

1. Introduction

In the last two decades, nanoplasmonics has experienced a huge impulse from both theoretical and experimental points of view. This branch of nanophotonics studies the distribution of the electromagnetic field, and its local charge resonances (Localized Surface Plasmon Resonances, LSPRs) in sub-wavelength metallic nanostructures. These SPRs localize and strongly enhance the incident field near the nanostructure at dimensions much smaller than its wavelength [1]. This phenomenon has been exploited for many applications in several scientific fields such as medicine [2], optical communications [3], spectroscopy [4], chemical sensing [5] or photocatalysis [6].

Many studies have analyzed how the LSPRs can be spectrally tuned by varying the shape, size and material of the nanoparticle, as well as its surrounding conditions [7]. Most of this research has been done in the visible and near-infrared ($\lambda > 400$ nm) where Au nanoparticles have played a leading role due to their oxide-free nature and biocompatibility.

Extending nanoplasmonics to the UV range has become a topic of interest due to the new challenges arising in specific areas. For example, many biological compounds, such as nucleotide bases, nucleic acids or aromatic amino acids in cells, have absorption bands in the UV (below $\lambda = 300$ nm) [8–10]. By using hot spots excited by LSPRs in the UV, it is possible to improve surface enhanced spectroscopy techniques (SERS [4], TERS [11], etc.) that ease the detection and recognition of these kinds of biomolecules. Also, biosensing assisted by LSPRs monitors the spectrum around the plasma resonance looking for shifts produced by changes in the extinction curves related to some target analyte. Bioimaging is another area that benefits from using UV radiation since the diffraction limit is proportional to the wavelength. Another example is photocatalysis, an area of research which has experienced a great development in the last decade. It has been recently discovered that metallic nanoparticles (NPs) are photocatalytically active, driving chemical reactions with photo-generated hot

carriers originated from the LSPRs' decay [6,12,13]. These hot carriers and their subsequent transfer to adsorbates can affect reactions pathways. By tuning the photon and LSPR energies so that hot carriers are injected into specific orbitals of reaction intermediates, product selectivity can be achieved. However, not all metals can be used for these kind of applications, only those with good plasmonic and catalytic behaviors.

As conventional metals such as Au or Ag cannot operate in the UV range due to the presence of interband transitions, several researches have analyzed possible new metallic alternatives in order to find those whose plasmonic performance could be suitable for the new challenges arising for photon energies above 3 eV [14,15]. Among the studied metals are aluminum (Al), gallium (Ga), indium (In), rhodium (Rh), ruthenium (Ru), tungsten (W), titanium (Ti), chromium (Cr), palladium (Pd), copper (Cu), platinum (Pt), and magnesium (Mg). Figure 1 shows the dimensionless Faraday number, *Fa* (or field-enhancement factor) [16] for different materials including all the above mentioned plus gold (Au), silver (Ag) and bismuth (Bi). Very recent results have presented Bi as a promising candidate for plasmonics in the UV range [17]. *Fa* quantifies and allows comparison of the ability of a material to enhance the electromagnetic field in the proximity of its surface. This expression has been proposed as a refinement to the plasmonic efficiency used in previous studies [14,15]. Figure 1 shows that Mg, Al, Ga and Rh present the highest value of *Fa* while having LSPRs in the UV. Although In also presents a value of *Fa* comparable to that of Ga, its oxidation process (5 nm vs 1 nm oxide shell thickness) prevents its application in the UV [14].

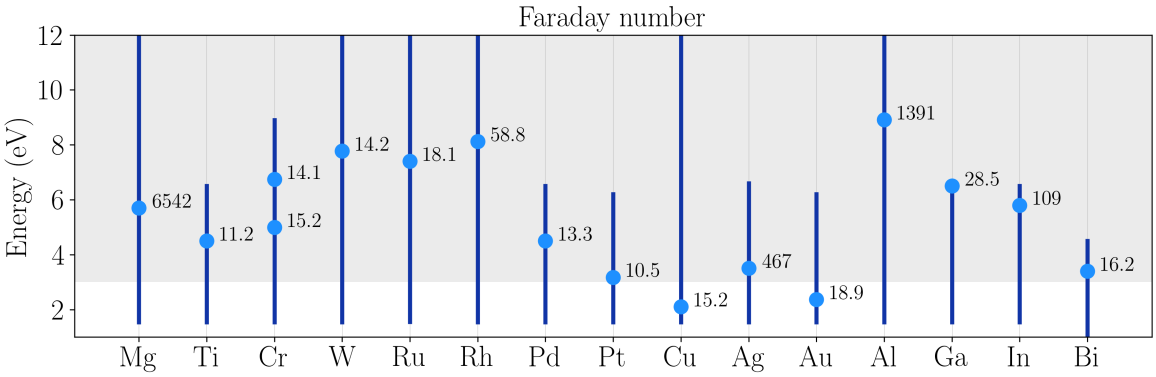

Figure 1. Faraday number (*Fa*) for different metals. The blue dot represents the resonant energy (Fröhlich frequency, frequency at which $Re(\epsilon) = -2$ [15]) and the shadowed region the exciting photon energies above 3 eV. The blue solid line represents the range of energies studied in each case (this depends on the optical constants available in the literature [17–20]).

The plasmonic performance of these metals depends on the surrounding dielectric environment. All of them, except Rh, form native oxides shells that wrap the NP and whose thickness highly depends on the exposure conditions: temperature and pressure. The thickness of this oxide shell can go from 1 nm, as in the case of Ga, to the complete destruction of the metal content of the NP, as in the case of Mg [21]. So, knowing how this oxide shell affects the plasmonic behavior of this type of NPs is a key point for researchers in UV plasmonics [22–24]. It will be addressed in the next two sections for the four most significant metals able to sustain UV LSPRs. It is worth mentioning that materials with UV plasmonic response can also be achieved by alloying elemental materials [25].

The review is organized as follows. Firstly, we will review the properties and related work on four metals with good plasmonic performance in the UV range. These metals have been divided in two different groups depending on their high/low oxidation tendency. Secondly, we will analyze the plasmonic response of NPs made of these materials with different shapes while considering their respective oxide shells. Finally, we present some examples of local-field cooperative effects in dimers.

2. High Oxidation Tendency: Aluminum and Magnesium

2.1. Aluminum

Aluminum is the third most abundant element in the Earth's crust, only behind oxygen and silicon. This makes it two to three orders of magnitude cheaper than other conventional plasmonic metals like Au or Ag. It presents a strong plasmonic response in the UV range, and unlike precious metals, its interband transitions lie in the near infra-red (NIR around 800 nm) [26]. For instance, Al is compatible with optoelectronic devices and complementary metal–oxide–semiconductor (CMOS) technology. Most importantly, there is a high number of processing methods for manufacturing Al NPs of different sizes and shapes [27]. Among these methods are lithography, laser ablation and chemical synthesis. This includes nanorods [28–30], nanodisks [22] or flat triangles [31,32]. The main disadvantage is its inherent high tendency to oxidation. When exposed to air, a thin layer of oxide wraps the NP [33]. Although the layer thickness is small (a few nanometers), it is highly sensitive to ambient conditions: temperature and humidity. As a consequence, plasmonic resonances of Al NPs are spectrally modified. It has been experimentally and theoretically shown that the growth of this oxide layer leads to both a red-shift and a weakening of the resonance peaks in Al NPs with different shapes [22,23,31,34]. On the other hand, the self terminating oxide layer can prevent further oxidation, producing a natural encapsulation. This is why this oxide layer is sometimes described as a "protective" layer. Recent experiments on Al nanorods, have shown that high-order resonant modes are more confined inside the oxide-shell [30].

Recently, a lot of attention has been paid to Al in photocatalysis applications. Traditionally, transition metals like Rh, Ru or Pd have been used in heterogeneous catalysis to lower the activation energy of chemical reactions. However, these metals present lower absorption and weaker LSPRs in the UV spectral region. This is a disadvantage for photocatalytic applications due to the poor overlap with either conventional lasers sources or the solar spectrum. For these reasons, it has been proposed to couple a plasmonic antenna directly to the catalytic nanoparticle. This antenna-reactor complex allows absorption enhancements in poorly light-absorbing catalytic metals [35]. The feasibility of these heterostructures has been demonstrated using Al as "antenna" and Pd as "reactor" heterodimers [35] and decorated spherical nanoparticles [36]. Aluminum-cuprous oxide antenna-reactor nanoparticles have also been proven to be an efficient photocatalytic heterostructure [37]. More recently, it has been reported the possibility of producing Al nanocrystals decorated with transition metal nanoislands [38]. These metals include among others Rh, Ru or Pd, which have already been used in heterogeneous catalysis. Although Al by itself is a poor catalytic metal, it has been demonstrated that Al nanocrystals can also act as photocatalysts for hydrogen dissociation [39]. Densely distributed Al NPs have been also used to assist photocatalytic processes [40,41].

Aluminum nanostructured films have been widely used as substrate for enhanced fluorescence spectroscopy in the UV for detection of biomolecules [42,43]. Al nanoapertures have been studied as a tool for the modification of fluorescence decay rate of p-terphenyl dye molecules [44,45]. Wang et al. [45] reported a lifetime reduction of $\approx$7.2$\times$, exceeding the previously reported value $\approx$3.5$\times$ by Jiao et al. [44]. The first fabrication of Al film-over substrate for UV surface-enhanced resonance Raman scattering at the deepest UV wavelength used to date (λ = 229 nm) [46] has been reported.

Ahmadivand et al. [47] have proposed to use aluminum nanoantennas to enhance the response of a GaN UV detector and, in this way, overcome some of the problems of current UV photodectors [48]. This nanoantenna consists on Al/Al_2O_3 heptamers with the symmetry of a benzene molecule as Fano-resonant plasmonic nanoclusters. Their results showed that these assemblies are able to generate hot electrons to enhance the absorption by inducing Fano-resonant modes across the UV spectral region.

2.2. Magnesium

Magnesium nanoparticles also present a strong plasmonic response in the UV, even stronger than Al. The efficiency of them is higher than those of Al for the same wavelength range. However,

the oxidation of Mg NPs is more aggressive. The native oxide MgO forms without stopping upon exposure to air as oxygen rapidly diffuses through porous oxide into the metal [15,23]. This process leads to a complete destruction of the plasmonic effects on Mg NPs, unless they are manipulated under controlled atmospheres [49]. In order to prevent their oxidation and preserve their UV plasmonic performance, a coating procedure with gallium has been recently proposed [50].

A very interesting fact about Mg is that it can absorb up to 7.6 wt % of hydrogen gas [51]. This, together with its abundance and low cost, makes Mg a very attractive material for hydrogen storage and hydrogen sensing purposes in the looming hydrogen economy [52,53]. Recently, it has been experimentally demonstrated how the plasmonic response of Mg NPs (more precisely, nanodisks fabricated by colloidal hole-mask lithography) can be switched from "on" to "off" states by exposing them to molecular hydrogen (H_2). Mg upon exposure to H_2 turns into MgH_2, which, as a dielectric material, does not support plasmonic resonances. The hydrogenation process is reversible by exposure to oxygen, turning MgH_2 into metallic Mg again [49]. This feature makes Mg very appealing for creating new active plasmonic devices. For example, this metal-dielectric transition has been experimentally used in the construction of an hybrid plasmonic metamolecule with hydrogen-regulated chiroptical response [54].

In the field of bio-sensing, the modification of the ultraviolet (UV) fluorescence decay rate of p-terphenyl dye molecules by Mg nanoapertures in free solution has been reported by Wang et al. [45]. Mg nanoapertures exhibit a lifetime reduction of up to $\approx 7.2\times$. This value is higher than that reported for Al ($\approx 5.3\times$). Single Mg nanohelices with strong chiroptical response have also been reported as plasmonic sensors for molecular detection [55].

3. Low Oxidation Tendency: Gallium and Rhodium

3.1. Gallium

Gallium is a standard material in optoelectronics that is becoming attractive also for its plasmonic properties. It presents a broad plasmon tunability, it is stable along a wide range of temperatures and its deposition is simple even at room temperature [24]. Moreover, the new range of bottom-up fabrications techniques that allow the production of Ga NPs, make this material very appealing for practical purposes. These fabrication methods include molecular beam epitaxy (MBE) [24,56], optically regulated self-assembly [57], thermal evaporation [58], and colloidal synthesis [59]. In addition, unlike either Al or Mg, its very low tendency to oxidation (1–2 nm oxide shell thickness), minimally affects its optical properties, keeping them stable over months or even years [23,24]. Ga NPs form liquid droplets with a melting point of 30 °C, so when deposited on a substrate at room temperature, they produce a close-packed array of smooth truncated spheres whose mean radii and size distributions vary with growth conditions. Wu et al. [56] presented the optical evolution of Ga NPs surface plasmon resonance during deposition by in situ ellipsometry to control and tune the plasmon resonance photon energy. This work reported both longitudinal and transverse modes for the hemispherical Ga NPs supported on a sapphire substrate. Similar results were obtained by Albella et al. [60] through a numerical study based on the Discrete Dipole Approximation (DDA) [61]. Other methods used to study this type of nanoparticles include variable-angle spectroscopic and Mueller matrix ellipsometry [62] or hyperspectral cathodoluminescence imaging [63].

The utility of these Ga NPs seeded substrates has been demonstrated for UV surface-enhanced Raman spectroscopy, fluorescence, and photodegradation, following excitation by a HeCd laser operating at 325 nm [64].

Other studies have explored the possibility of alloying or coating these Ga NPs with other metals such as Mg. Wu et al. [65] experimentally analyzed the plasmonic properties of this type of NPs. These bimetallic NPs allow a new degree of freedom for tuning the LSPRs since their optical constants are dependent on the mixture composition. The resulting Ga-Mg NPs exhibit a plasmon

resonance tunable from the UV to the IR by playing with the particle size and the Ga/Mg ratio [50]. Electromagnetic simulations based on DDA numerically corroborated these experimental results [50].

Very recently, it was experimentally shown, through real-time ellipsometry, the stable coexistence of a solid-phase core and a liquid shell in substrate-supported Ga NPs [20]. Both liquid and solid phases present significantly different optical properties [20]. While the liquid phase presents a Drude-like dielectric function, the solid phase presents interband transitions in the 2.19–2.40 eV range. This fact is relevant for plasmonic applications, since the plasmonic performance of metallic NPs is very sensitive to their optical properties.

Krasavin et al. [66] proposed a new concept for active plasmonics that exploits light-induced nanoscale structural transformations in the waveguide material. Specifically, they showed that surface plasmon polaritons signals in a metal-on-dielectric waveguide containing a Ga section a few microns long can be effectively controlled by switching the structural phase of gallium. They were able to induced the phase change by thermal or optical excitation. Taking advantage of the gallium's solid-liquid phase transition, Vivekchand et al. [67] fabricated liquid Ga gratings which exhibited reversible and switchable phase-dependent plasmonic properties. The liquid phase showed higher surface plasmon polaritons coupling efficiencies and narrower resonance line widths compared to the solid phase. In order to predict the optical constants of liquid metals and metal alloys, Blaber et al. [68] proposed a density functional theory molecular dynamics model that allows to calculate them from first principles with no a priori knowledge of the system. This method was tested on liquid Ga and In-Ga eutectic alloy.

3.2. Rhodium

Although Ga NPs form an oxide shell only 1–2 nm thick, oxide-free metals, like Pd, Pt, Ru or Rh, should be even more desirable. Of all these noble metals, Rh presents the strongest plasmonic response in the UV range. Moreover, the possibility of synthesizing Rh NP with sizes smaller than 10 nm through chemical methods [69,70] and its potential for photocatalytic applications, makes this material very attractive for building plasmonic tools in which photon energies are well above 3 eV [69]. As a disadvantage, Rh is less abundant than metals like Al or Mg. This fact has a logical impact on the price: the price of Rh is more than 10^4 higher than that of Al or Mg.

In our previous research, two different Rh NP have been synthesized: tripod stars [69,71] and nanocubes [70]. On the one hand, Watson et al. [69] synthesized and experimentally examined the properties of Rh tripods by means of SERS, surface enhanced fluorescence, and photoinduced degradation of a typical compound like p-aminothiophenol (PATP). They found that Raman and fluorescence spectra were enhanced and photodegradation was accelerated in the presence of Rh under resonant UV excitation. In addition they observed that for more tightly focused UV illumination, fluorescence spectra often increased for many minutes. This is an indication that photo-excited hot electrons efficiently transferred from the Rh NPs to the attached PATP before photodamage ultimately quenched the fluorescence. These efficient photodegradation and photo-induced charge transfer processes confirmed the potential of Rh nanostructures for UV plasmonic and photocatalytic applications. On the other hand, a similar study was carried out by Zhang et al. [70]. They were able to synthesize uniform Rh NCs with controlled side length ranging between 10 to 59 nm. They observed that the UV LSPRs of the NCs accelerated the rate of PATP chemical decomposition.

Rh has also been presented as a promising metal for plasmonic photocatalysis. Supported Rh nanoparticles and molecular complexes are widely used in industrial hydrogenation, hydroformylation and ammonia oxidation reactions. However, its main industrial application is in three-way catalytic converters to reduce NO_x, where Rh is often alloyed with Pt and Pd because of its corrosion resistance [72–74]. Very recently, Zhang et al. [75] reported that plasmonic Rh nanoparticles are photocatalytic, simultaneously lowering activation energies and exhibiting strong product photo-selectivity, as illustrated through the CO_2 hydrogenation reaction. These results have opened

an exciting new pathway in the long history of heterogeneous catalysis by offering a compelling advantage of light over heat.

The plasmonic response of a nanoparticle is very dependent on the shape of the nanostructure [7]. Through chemical synthesis and repeated use in photocatalytic processes, some defects may appear on the NPs. For example, in the case of the NCs, they present rounded edges and some concavities/convexities on the faces as it is shown in TEM images [70,75]. In fact, it has been demonstrated that the concavity of Rh nanocubes can be controlled by using a site-selective etching strategy [76]. The effect that these deviations from the perfect shape has on the plasmonic performance has been studied by Gutiérrez et al. [77].

Other authors have proposed to used Rh nanoparticles for deep-UV bio-chemical sensing [78]. They proposed nanostructures composed of nanorings dimer-type antennas and an infinity shape structure built by a pair of split rings with a nanodisk. These nanostructures support Fano resonances that can be used for deep-UV biochemical sensing applications.

4. Comparison of the Plasmonic Response of Simple Geometries: Oxidation Effects

In this section, we will compare the plasmonic response in both the near- and far-field regimes of nanostructures made of Al, Mg, Ga and Rh. The parameter of interest in the far-field regime will be the absorption cross-section C_{abs}, while for the near-field we calculate the enhancement of the local intensity averaged over the NP surface $\langle |E|^2 \rangle$. From now on, we will refer to $\langle |E|^2 \rangle$ as *averaged local enhancement* for brevity. In the case of Al, Mg and Ga, NPs will be modeled with an oxide thickness of 3, 5 and 1 nm, respectively, to be consistent with previous numerical and experimental studies [20,22,49].

Figure 2 shows the complex dielectric permittivity ($\epsilon = \epsilon_r + i\epsilon_i$) of these metals and their corresponding oxides. The values of the complex dielectric permittivity have been taken from different sources in the literature [18,20,79]. Note the similar optical behavior shown by Mg and Al oxides, while Ga_2O_3 shows absorption in the UV region above 3 eV.

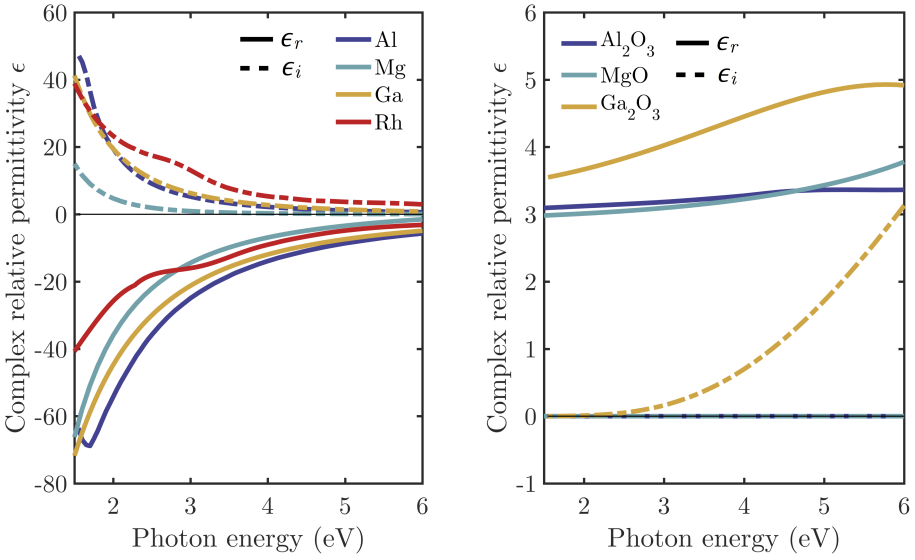

Figure 2. Real (solid line) and imaginary (dashed line) parts of the complex relative permittivity ($\epsilon = \epsilon_r + i\epsilon_i$) of Al, Mg, Ga, Rh (**left**) and their corresponding oxides (**right**) as a function of the photon energy of the incident beam. The values of the complex relative permittivities have been taken from different sources from the literature [18,20,79].

As in a previous work [80], we have considered tripod stars ($l = 10$ nm, $w = 5$ nm and $h = 5$ nm), cubes ($L = 8.1139$ nm) and spheres ($R = 5.0335$ nm) with equivalent volume. By choosing nanoparticles with the same volume but different shape, it is possible to explore the relative contribution of the

shape (corners and edges effects included) and the material. Such small NPs are highly demanded in photocatalysis applications. It is well known that small NPs have higher catalytic activity than larger ones due to their increased surface to volume ratio. The hot-electrons produced by LSPR excitation in these small NPs are more likely to reach the surface and enter anti-bonding orbitals of adsorbed molecules, thereby weakening a critical bond and accelerating the reaction [38].

Figure 3 shows the absorption cross-section C_{abs} (top row) and averaged local enhancement $\langle|E|^2\rangle$ (bottom row) for equivalent tripod stars, spheres, and cubes made of Al + Al_2O_3, Mg + MgO, Ga + Ga_2O_3 and Rh. The oxide shell thickness in each case has been set to 3, 5 and 1 nm respectively [22,24,49]. The aforementioned dimensions for the tripod stars, cubes and spheres already include the thickness of oxide shell in each case. The percentage of metal content in each nanoparticle is shown in Table 1. This magnitude is defined as $V(metal)/V(metal + oxide) \times 100$, where V represents the volume of either metal or metal+oxide within the NP.

Table 1. Percentage of metal content in each of the studied nanoparticles.

Metal	Tripod Star	Cube	Sphere
Al + Al_2O_3	0%	1.8%	6.6%
Mg + MgO	0%	0%	0%
Ga + Ga_2O_3	22%	42%	51%
Rh	100%	100%	100%

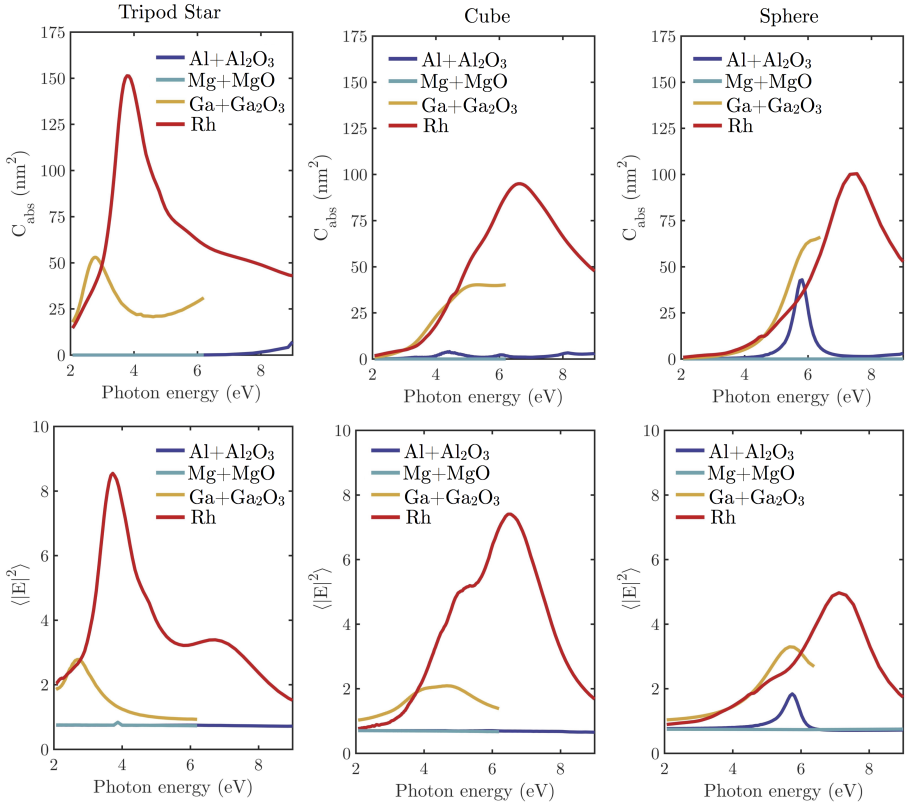

Figure 3. Spectral enhancement of the local intensity averaged over the NP surface $\langle|E|^2\rangle$ (left column) and the absorption cross-section C_{abs} for equivalent tripod stars (l = 10 nm; $w = h$ = 5 nm), cubes (L = 8.1139 nm) and spheres (R = 5.0335 nm) composed of Al + Al_2O_3, Mg + MgO, Ga + Ga_2O_3 and Rh, illuminated under normal incidence.

Figure 4 shows the $|E|^2$ maps (logarithmic scale) at E = 3.82 eV (λ = 325 nm, HeCd laser) for Rh and Ga + Ga_2O_3 tripod stars (l = 10 nm, w = 5 nm and h = 5 nm), nanocubes (L = 8.1139 nm) and

spheres (R = 5.0335 nm). These two materials have been chosen in order to show how the near-field distribution is affected by the presence of an oxide shell. A deep analysis of this topic on Al + Al_2O_3, Mg + MgO and Ga + Ga_2O_3 spherical and hemispherical geometries was made by Gutiérrez et al. [23].

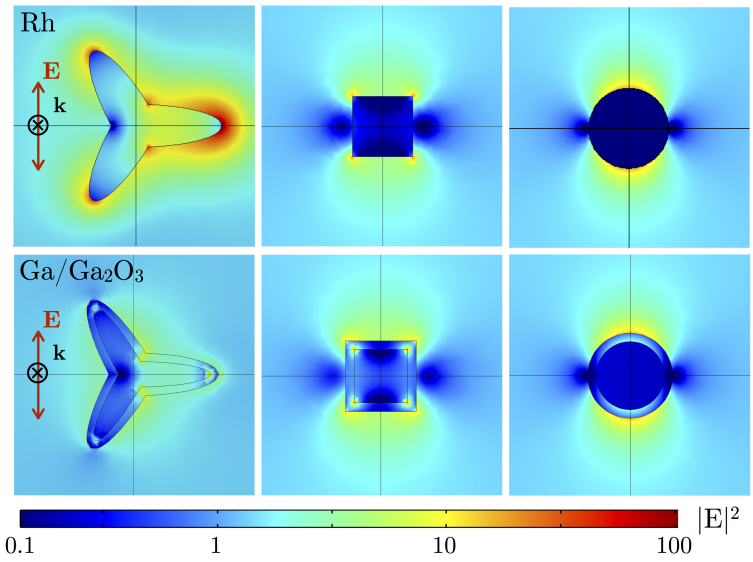

Figure 4. $|E|^2$ maps (logarithmic scale) at E = 3.82 eV (λ = 325 nm, HeCd laser) for Rh (top row) and Ga + Ga_2O_3 (bottom row) tripod stars (l = 10 nm; $w = h$ = 5 nm), cubes (L = 8.1139 nm) and spheres (R = 5.0335 nm).

The plasmonic response of Al and Mg is completely deteriorated by the formation of the oxide layer, specially in the case of Mg, for which the metal content drops to 0% after oxidation. This aggressive oxidation process limits the performance of Mg NPs with sizes smaller than 10 nm. It is surprising how the absorption cross section of the Al sphere (with a metal content of just 1.8%) is comparable to that of Ga and Rh spheres at energies around 6 eV. However, when looking at the value of $\langle|E|^2\rangle$, for Al spherical NPs, it is approximately half the value for Rh and Ga spherical ones.

By comparing Ga and Rh (low oxidizing tendency), in general, the former presents LSPRs at lower energies than the latter (coherent with their Fröhlich frequencies, 6.5 and 8.1 eV, respectively). Moreover, for energies above 3 eV both C_{abs} and $\langle|E|^2\rangle$ are higher for Rh NPs than for Ga NPs. The only exception occurs for the sphere geometry, for which Ga presents higher absorption and electric field enhancement between 5 and 6 eV approximately. From this comparison, it can be concluded that oxidation prevents Al and Mg to be optimum candidates as plasmonic materials. On the contrary, Ga and Rh show a good plasmonic response, specially Rh, which presents almost highest values of C_{abs} and $\langle|E|^2\rangle$ all over the studied spectral range.

Electric field hot-spots can be observed in specific locations for each geometry (see Figure 4). Also, the effect that oxide shells have on them is shown in the bottom row for Ga + Ga_2O_3 NPs. In absence of oxide, hot-spots are produced on the surface of the particle, where they can be in direct contact with the analytes in surface enhanced applications. When an oxide shell is present, for very thin shells and specific geometries, hot-spots produced on the surface of the oxide are more intense than those at the interface metal-oxide (see the Ga + Ga_2O_3 sphere). However, for other geometries like Ga + Ga_2O_3 tripod stars and nanocubes, hot-spots produced in the metal-oxide boundary are more intense. So, as for the case of Ga, the oxide shell can have a critical effect on the UV plasmonic performance of metallic nanostructures and its relevance to real applications.

Finally, it is important to point out that, although Rh in principle presents not as good plasmonic properties as Al or Mg (lower Fa, see Figure 1), because its does not oxidize, its plasmonic response is more adequate for practical purposes.

5. Cooperative Effects: Dimer Induced Hot-Spots

In this section we will compare cooperative effects in Rh tripod star and nanocube dimers since these are two of the synthesizable geometries, and also, because the absence of an oxide-shell makes this material very appealing for UV applications. In particular, we will explore the strong interaction region between metallic NP dimers, where single molecules have been detected with other metals [81,82]. The studied interparticle distance (gaps) ranges between 1 and 10 nm. The shortest gap has been chosen to be 1 nm in order to avoid quantum tunneling effects between particles [83] (the electron tunneling transmission vanishes when the gap is larger than ≈ 0.8 nm [84]).

Figure 5 plots (a) the near-field intensity $|E|^2$ maps at E = 3.82 eV (λ = 325 nm, HeCd laser), (b) the maximum value of the near-field intensity at the center of the gap, and (c) the absorption cross-section C_{abs} spectra as a function of the gap spacing for tripod stars (left) and nanocubes (right) dimers under normal incidence illumination and polarization parallel to the dimer axis. It can be pointed out that as the gap becomes smaller, the value of C_{abs} increases and so does the near-field intensity at the center of the gap for both geometries. Also, the peak of C_{abs} is blue-shifted. This behavior is in perfect agreement with results reported by Rechberger et al. [85].

Nevertheless, since the plasmonic response is very dependent on the nanoparticle's shape, tripod star and nanocube dimers behave very differently. The LSPR peak corresponding to the nanocube dimer is ≈2.5 eV blue-shifted with respect to that of the tripod star. Moreover, the latter present larger values of C_{abs} than the former. By looking at the maximum near-field enhancement at the center of the gap, the tripod star dimer presents in hot-spot a value of $|E|^2$ around one order of magnitude higher than that of the nanocube for shorter gaps. This can be understood in terms of the lightning rod effect [86] since the tripod star dimer gap is between two sharp tips instead of between two flat surfaces (nanocube dimer). However, for the larger gaps, the near-field enhancement takes very similar values. Therefore, the near-field enhancement at the center of the gap decays faster with increasing interparticle distance for the tripod star dimer.

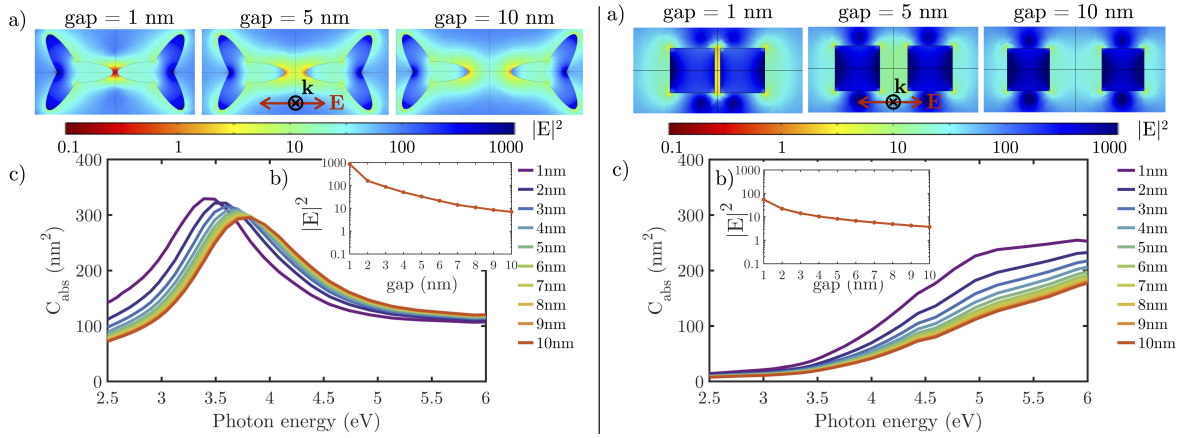

Figure 5. (**a**) Logarithmic scale $|E|^2$ maps at E = 3.82 eV (λ = 325 nm, HeCd laser), (**b**) maximum near-field enhancement at the center of the gap and (**c**) spectral absorption cross-section Cabs for tripod star (**left**) and nanocubes (**right**) dimers of several gaps, varying from 1 to 10 nm, illuminated under normal incidence with polarization parallel to the dimer axis.

6. Conclusions

UV plasmonics constitutes a new focus of research due to new challenges arising in fields such as biology, chemistry or spectroscopy. In our quest to find suitable metals for the UV range, we have analyzed recent work developed for four metals that present plasmonic behavior in this spectral region: aluminum, magnesium, gallium and rhodium. These metals have been classified into two categories: those with high oxidation tendency (Al and Mg) and those with low oxidation tendency (Ga and Rh).

By comparing the plasmonic response of small NPs (sizes smaller than 10 nm) made of these metals with their corresponding oxide layers, it can be concluded that the plasmonic performance of Al and Mg NPs is strongly affected by an oxide layer. This weakens their absorption efficiency and near-field enhancement. This effect is less noticeable as the size of the particle increases, specially for Al, which forms a self-terminating oxide shell. Recently, Rh, an oxide-free metal, has drawn the attention because it enhances its already favorable catalytic activity by UV illumination near its plasmonic resonance. From the experimental point of view, two geometries can be chemically synthesized: tripod stars and nanocubes. Rhodium NPs have shown the best UV plasmonic performance as compared with the other metals (highest values of absorption cross-section and near-field enhancement, specially on those geometries with edges and corners). In this review, we have also analyzed cooperative effects on dimers of Rh nanoparticles for those two geometries.

Acknowledgments: This research has been supported by MICINN (Spanish Ministry of Science and Innovation, project FIS2013-45854-P) and sponsored by the Army Research Laboratory and was accomplished under Cooperative Agreement Number W911NF-17-2-0023. Y.G. wants to thank the University of Cantabria for her FPU grant.

Author Contributions: Y.G., D.O., R.A.d.l.O., J.M.S., F.G. and F.M. conceived the original idea. Y.G. and R.A.d.l.O. carried out numerical calculations. Y.G., D.O., R.A.d.l.O., J.M.S., F.G. and F.M. analyzed the results and figures. Y.G. wrote the paper. F.M. supervised the study. All authors reviewed the manuscript.

Conflicts of Interest: The authors declare no conflict of interest.

References

1. Prasad, P.N. *Nanophotonics*; John Wiley & Sons, Inc.: Hoboken, NJ, USA, 2004.
2. Aslan, K.; Lakowicz, J.R.; Geddes, C.D. Plasmon light scattering in biology and medicine: New sensing approaches, visions and perspectives. *Curr. Opin. Chem. Biol.* **2005**, *9*, 538–544.
3. Ozbay, E. Plasmonics: Merging Photonics and Electronics at Nanoscale Dimensions. *Science* **2006**, *311*, 189–193.
4. Sharma, B.; Frontiera, R.R.; Henry, A.I.; Ringe, E.; Van Duyne, R.P. SERS: Materials, applications, and the future. *Mater. Today* **2012**, *15*, 16–25.
5. Anker, J.N.; Hall, W.P.; Lyandres, O.; Shah, N.C.; Zhao, J.; Van Duyne, R.P. Biosensing with plasmonic nanosensors. *Nat. Mater.* **2008**, *7*, 442–453.
6. Kale, M.J.; Avanesian, T.; Christopher, P. Direct photocatalysis by plasmonic nanostructures. *ACS Catal.* **2014**, *4*, 116–128.
7. Noguez, C. Surface plasmons on metal nanoparticles: The influence of shape and physical environment. *J. Phys. Chem. C* **2007**, *111*, 3606–3619.
8. Voet, D.; Gratzer, W.B.; Cox, R.A.; Doty, P. Absorption spectra of nucleotides, polynucleotides, and nucleic acids in the far ultraviolet. *Biopolymers* **1963**, *1*, 193–208.
9. Kumamoto, Y.; Taguchi, A.; Smith, N.I.; Kawata, S. Deep UV resonant Raman spectroscopy for photodamage characterization in cells. *Biomed. Opt. Express* **2011**, *2*, 927.
10. Kumamoto, Y.; Taguchi, A.; Smith, N.I.; Kawata, S. Deep ultraviolet resonant Raman imaging of a cell. *J. Biomed. Opt.* **2012**, *17*, 0760011.
11. Taguchi, A. Plasmonic tip for nano Raman microcopy: Structures, materials, and enhancement. *Opt. Rev.* **2017**, *24*, 462–469.
12. Linic, S.; Aslam, U.; Boerigter, C.; Morabito, M. Photochemical transformations on plasmonic metal nanoparticles. *Nat. Mater.* **2015**, *14*, 567–576.
13. Christopher, P.; Moskovits, M. Hot Charge Carrier Transmission from Plasmonic Nanostructures. *Ann. Rev. Phys. Chem.* **2017**, *68*, 379–398.
14. McMahon, J.M.; Schatz, G.C.; Gray, S.K. Plasmonics in the ultraviolet with the poor metals Al, Ga, In, Sn, Tl, Pb, and Bi. *Phys. Chem. Chem. Phys.* **2013**, *15*, 5415–5423.
15. Sanz, J.M.; Ortiz, D.; Alcaraz de la Osa, R.; Saiz, J.M.; González, F.; Brown, A.S.; Losurdo, M.; Everitt, H.O.; Moreno, F. UV Plasmonic Behavior of Various Metal Nanoparticles in the Near- and Far-Field Regimes: Geometry and Substrate Effects. *J. Phys. Chem. C* **2013**, *117*, 19606–19615.

16. Lalisse, A.; Tessier, G.; Plain, J.; Baffou, G. Quantifying the Efficiency of Plasmonic Materials for Near-Field Enhancement and Photothermal Conversion. *J. Phys. Chem. C* **2015**, *119*, 25518–25528.
17. Toudert, J.; Serna, R.; Camps, I.; Wojcik, J.; Mascher, P.; Rebollar, E.; Ezquerra, T.A. Unveiling the Far Infrared-to-Ultraviolet Optical Properties of Bismuth for Applications in Plasmonics and Nanophotonics. *J. Phys. Chem. C* **2017**, *121*, 3511–3521.
18. Palik, E.D. *Handbook of Optical Constants of Solids*; Academic Press: Cambridge, MA, USA, 1998.
19. Johnson, P.B.; Christy, R.W. Optical Constants of the Noble Metals. *Phys. Rev. B* **1972**, *6*, 4370–4379.
20. Losurdo, M.; Suvorova, A.; Rubanov, S.; Hingerl, K.; Brown, A.S. Thermally stable coexistence of liquid and solid phases in gallium nanoparticles. *Nat. Mater.* **2016**, *15*, 995–1002.
21. Fournier, V.; Marcus, P.; Olefjord, I. Oxidation of magnesium. *Surf. Interface Anal.* **2002**, *34*, 494–497.
22. Knight, M.W.; King, N.S.; Liu, L.; Everitt, H.O.; Nordlander, P.; Halas, N.J. Aluminum for plasmonics. *ACS Nano* **2014**, *8*, 834–840.
23. Gutierrez, Y.; Ortiz, D.; Sanz, J.M.; Saiz, J.M.; Gonzalez, F.; Everitt, H.O.; Moreno, F. How an oxide shell affects the ultraviolet plasmonic behavior of Ga, Mg, and Al nanostructures. *Opt. Express* **2016**, *24*, 20621.
24. Wu, P.C.; Khoury, C.G.; Kim, T.H.; Yang, Y.; Losurdo, M.; Bianco, G.V.; Vo-Dinh, T.; Brown, A.S.; Everitt, H.O. Demonstration of Surface-Enhanced Raman Scattering by Tunable, Plasmonic Gallium Nanoparticles. *J. Am. Chem. Soc.* **2009**, *131*, 12032–12033.
25. Gong, C.; Leite, M.S. Noble Metal Alloys for Plasmonics. *ACS Photonics* **2016**, *3*, 507–513.
26. DeSantis, C.J.; McClain, M.J.; Halas, N.J. Walking the Walk: A Giant Step toward Sustainable Plasmonics. *ACS Nano* **2016**, *10*, 9772–9775.
27. Martin, J.; Plain, J. Fabrication of aluminium nanostructures for plasmonics. *J. Phys. D Appl. Phys.* **2015**, *48*, 184002.
28. Ekinci, Y.; Solak, H.H.; Löffler, J.F. Plasmon resonances of aluminum nanoparticles and nanorods. *J. Appl. Phys.* **2008**, *104*, 083107.
29. Knight, M.W.; Liu, L.; Wang, Y.; Brown, L.; Mukherjee, S.; King, N.S.; Everitt, H.O.; Nordlander, P.; Halas, N.J. Aluminum plasmonic nanoantennas. *Nano Lett.* **2012**, *12*, 6000–6004.
30. Martin, J.; Kociak, M.; Mahfoud, Z.; Proust, J.; Gérard, D.; Plain, J. High-resolution imaging and spectroscopy of multipolar plasmonic resonances in aluminum nanoantennas. *Nano Lett.* **2014**, *14*, 5517–5523.
31. Chan, G.H.; Zhao, J.; Schatz, G.C.; Duyne, R.P.V. Localized surface plasmon resonance spectroscopy of triangular aluminum nanoparticles. *J. Phys. Chem. C* **2008**, *112*, 13958–13963.
32. Campos, A.; Arbouet, A.; Martin, J.; Gérard, D.; Proust, J.; Plain, J.; Kociak, M. Plasmonic Breathing and Edge Modes in Aluminum Nanotriangles. *ACS Photonics* **2017**, *4*, 1257–1263.
33. Rai, A.; Park, K.; Zhou, L.; Zachariah, M.R. Understanding the mechanism of aluminium nanoparticle oxidation. *Combust. Theory Model.* **2006**, *10*, 843–859.
34. Langhammer, C.; Schwind, M.; Kasemo, B.; Zoric, I. Localized surface plasmon resonances in aluminum nanodisks. *Nano Lett.* **2008**, *8*, 1461–1471.
35. Zhang, C.; Zhao, H.; Zhou, L.; Schlather, A.E.; Dong, L.; McClain, M.J.; Swearer, D.F.; Nordlander, P.; Halas, N.J. Al–Pd Nanodisk Heterodimers as Antenna–Reactor Photocatalysts. *Nano Lett.* **2016**, *16*, 6677–6682.
36. Swearer, D.F.; Zhao, H.; Zhou, L.; Zhang, C.; Robatjazi, H.; Martirez, J.M.P.; Krauter, C.M.; Yazdi, S.; McClain, M.J.; Ringe, E.; et al. Heterometallic antenna-reactor complexes for photocatalysis. *Proc. Natl. Acad. Sci. USA* **2016**, *113*, 8916–8920.
37. Robatjazi, H.; Zhao, H.; Swearer, D.F.; Hogan, N.J.; Zhou, L.; Alabastri, A.; McClain, M.J.; Nordlander, P.; Halas, N.J. Plasmon-induced selective carbon dioxide conversion on earth-abundant aluminum-cuprous oxide antenna-reactor nanoparticles. *Nat. Commun.* **2017**, *8*, doi:10.1038/s41467-017-00055-z.
38. Swearer, D.F.; Leary, R.K.; Newell, R.; Yazdi, S.; Robatjazi, H.; Zhang, Y.; Renard, D.; Nordlander, P.; Midgley, P.A.; Halas, N.J.; et al. Transition-Metal Decorated Aluminum Nanocrystals. *ACS Nano* **2017**, 11, 10281–10288.
39. McClain, M.J.; Schlather, A.E.; Ringe, E.; King, N.S.; Liu, L.; Manjavacas, A.; Knight, M.W.; Kumar, I.; Whitmire, K.H.; Everitt, H.O.; et al. Aluminum Nanocrystals. *Nano Lett.* **2015**, *15*, 2751–2755.
40. Honda, M.; Kumamoto, Y.; Taguchi, A.; Saito, Y.; Kawata, S. Plasmon-enhanced UV photocatalysis. *Appl. Phys. Lett.* **2014**, *104*, 061108.

41. Honda, M.; Kumamoto, Y.; Taguchi, A.; Saito, Y.; Kawata, S. Efficient UV photocatalysis assisted by densely distributed aluminum nanoparticles. *J. Phys. D Appl. Phys.* **2015**, *48*, 184006.
42. Ray, K.; Chowdhury, M.H.; Lakowicz, J.R. Aluminum nanostructured films as substrates for enhanced fluorescence in the ultraviolet-blue spectral region. *Anal. Chem.* **2007**, *79*, 6480–6487.
43. Chowdhury, M.H.; Ray, K.; Gray, S.K.; Pond, J.; Lakowicz, J.R. Aluminum nanoparticles as substrates for metal-enhanced fluorescence in the ultraviolet for the label-free detection of biomolecules. *Anal. Chem.* **2009**, *81*, 1397–1403.
44. Jiao, X.; Peterson, E.M.; Harris, J.M.; Blair, S. UV Fluorescence Lifetime Modification by Aluminum Nanoapertures. *ACS Photonics* **2014**, *1*, 1270–1277.
45. Wang, Y.; Peterson, E.M.; Harris, J.M.; Appusamy, K.; Guruswamy, S.; Blair, S. Magnesium as a Novel UV Plasmonic Material for Fluorescence Decay Rate Engineering in Free Solution. *J. Phys. Chem. C* **2017**, *121*, 11650–11657.
46. Sharma, B.; Cardinal, M.F.; Ross, M.B.; Zrimsek, A.B.; Bykov, S.V.; Punihaole, D.; Asher, S.A.; Schatz, G.C.; Van Duyne, R.P. Aluminum Film-Over-Nanosphere Substrates for Deep-UV Surface-Enhanced Resonance Raman Spectroscopy. *Nano Lett.* **2016**, *16*, 7968–7973.
47. Ahmadivand, A.; Sinha, R.; Vabbina, P.K.; Karabiyik, M.; Kaya, S.; Pala, N. Hot electron generation by aluminum oligomers in plasmonic ultraviolet photodetectors. *Opt. Express* **2016**, *24*, 13665.
48. Li, D.; Sun, X.; Song, H.; Li, Z.; Chen, Y.; Jiang, H.; Miao, G. Realization of a high-performance GaN UV detector by nanoplasmonic enhancement. *Adv. Mater.* **2012**, *24*, 845–849.
49. Sterl, F.; Strohfeldt, N.; Walter, R.; Griessen, R.; Tittl, A.; Giessen, H. Magnesium as Novel Material for Active Plasmonics in the Visible Wavelength Range. *Nano Lett.* **2015**, *15*, 7949–7955.
50. Wu, P.C.; Losurdo, M.; Kim, T.H.; Garcia-Cueto, B.; Moreno, F.; Bruno, G.; Brown, A.S. Ga-Mg Core-shell nanosystem for a novel full color plasmonics. *J. Phys. Chem. C* **2011**, *115*, 13571–13576.
51. Zaluska, A.; Zaluski, L.; Ström-Olsen, J. Nanocrystalline magnesium for hydrogen storage. *J. Alloys Compd.* **1999**, *288*, 217–225.
52. Schlapbach, L.; Züttel, A. Hydrogen-storage materials for mobile applications. *Nature* **2001**, *414*, 353–358.
53. Wadell, C.; Syrenova, S.; Langhammer, C. Plasmonic Hydrogen Sensing with Nanostructured Metal Hydrides. *ACS Nano* **2014**, *8*, 11925–11940.
54. Duan, X.; Kamin, S.; Sterl, F.; Giessen, H.; Liu, N. Hydrogen-Regulated Chiral Nanoplasmonics. *Nano Lett.* **2016**, *16*, 1462–1466.
55. Jeong, H.H.; Mark, A.G.; Fischer, P. Magnesium plasmonics for UV applications and chiral sensing. *Chem. Commun.* **2016**, *52*, 12179–12182.
56. Wu, P.C.; Kim, T.H.; Brown, A.S.; Losurdo, M.; Bruno, G.; Everitt, H.O. Real-time plasmon resonance tuning of liquid Ga nanoparticles by in situ spectroscopic ellipsometry. *Appl. Phys. Lett.* **2007**, *90*, 103119.
57. MacDonald, K.F.; Fedotov, V.A.; Pochon, S.; Ross, K.J.; Stevens, G.C.; Zheludev, N.I.; Brocklesby, W.S.; Emel'yanov, V.I. Optical control of gallium nanoparticle growth. *Appl. Phys. Lett.* **2002**, *80*, 1643–1645.
58. Ghigna, P.; Spinolo, G.; Parravicini, G.B.; Stella, A.; Migliori, A.; Kofman, R. Metallic versus covalent bonding: Ga nanoparticles as a case study. *J. Am. Chem. Soc.* **2007**, *129*, 8026–8033.
59. Yarema, M.; Wörle, M.; Rossell, M.D.; Erni, R.; Caputo, R.; Protesescu, L.; Kravchyk, K.V.; Dirin, D.N.; Lienau, K.; von Rohr, F.; et al. Monodisperse Colloidal Gallium Nanoparticles: Synthesis, Low Temperature Crystallization, Surface Plasmon Resonance and Li-Ion Storage. *J. Am. Chem. Soc.* **2014**, *136*, 12422–12430.
60. Albella, P.; Garcia-Cueto, B.; González, F.; Moreno, F.; Wu, P.C.; Kim, T.H.; Brown, A.; Yang, Y.; Everitt, H.O.; Videen, G. Shape matters: Plasmonic nanoparticle shape enhances interaction with dielectric substrate. *Nano Lett.* **2011**, *11*, 3531–3537.
61. Draine, B.T.; Flatau, P.J. Discrete-dipole approximation for scattering calculations. *J. Opt. Soc. Am. A* **1994**, *11*, 1491–1499.
62. Yang, Y.; Akozbek, N.; Kim, T.h.; Sanz, J.M.; Moreno, F.; Losurdo, M.; Brown, A.S.; Everitt, H.O. Ultraviolet-Visible Plasmonic Properties of Gallium Nanoparticles Investigated by Variable-Angle Spectroscopic and Mueller Matrix Ellipsometry. *ACS Photonics* **2014**, *1*, 582–589.
63. Knight, M.W.; Coenen, T.; Yang, Y.; Brenny, B.J.M.; Losurdo, M.; Brown, A.S.; Everitt, H.O.; Polman, A. Gallium Plasmonics: Deep Subwavelength Spectroscopic Imaging of Single and Interacting Gallium Nanoparticles. *ACS Nano* **2015**, *9*, 2049–2060.

64. Yang, Y.; Callahan, J.M.; Kim, T.H.; Brown, A.S.; Everitt, H.O. Ultraviolet nanoplasmonics: A demonstration of surface-enhanced raman spectroscopy, fluorescence, and photodegradation using gallium nanoparticles. *Nano Lett.* **2013**, *13*, 2837–2841.
65. Wu, P.C.; Kim, T.H.; Suvorova, A.; Giangregorio, M.; Saunders, M.; Bruno, G.; Brown, A.S.; Losurdo, M. GaMg Alloy Nanoparticles for Broadly Tunable Plasmonics. *Small* **2011**, *7*, 751–756.
66. Krasavin, A.V.; Zayats, A.V.; Zheludev, N.I. Active control of surface plasmon–polariton waves. *J. Opt. A Pure Appl. Opt.* **2005**, *7*, S85–S89.
67. Vivekchand, S.R.C.; Engel, C.J.; Lubin, S.M.; Blaber, M.G.; Zhou, W.; Suh, J.Y.; Schatz, G.C.; Odom, T.W. Liquid Plasmonics: Manipulating Surface Plasmon Polaritons via Phase Transitions. *Nano Lett.* **2012**, *12*, 4324–4328.
68. Blaber, M.G.; Engel, C.J.; Vivekchand, S.R.C.; Lubin, S.M.; Odom, T.W.; Schatz, G.C. Eutectic Liquid Alloys for Plasmonics: Theory and Experiment. *Nano Lett.* **2012**, *12*, 5275–5280.
69. Watson, A.M.; Zhang, X.; Alcaraz de la Osa, R.; Marcos Sanz, J.; González, F.; Moreno, F.; Finkelstein, G.; Liu, J.; Everitt, H.O. Rhodium nanoparticles for ultraviolet plasmonics. *Nano Lett.* **2015**, *15*, 1095–1100.
70. Zhang, X.; Li, P.; Barreda, Á.; Gutiérrez, Y.; González, F.; Moreno, F.; Everitt, H.O.; Liu, J. Size-tunable rhodium nanostructures for wavelength-tunable ultraviolet plasmonics. *Nanoscale Horiz.* **2016**, *1*, 75–80.
71. Zettsu, N.; McLellan, J.M.; Wiley, B.; Yin, Y.; Li, Z.Y.; Xia, Y. Synthesis, Stability, and Surface Plasmonic Properties of Rhodium Multipods, and Their Use as Substrates for Surface-Enhanced Raman Scattering. *Angew. Chem. Int. Ed.* **2006**, *45*, 1288–1292.
72. Xie, S.; Liu, X.Y.; Xia, Y. Shape-controlled syntheses of rhodium nanocrystals for the enhancement of their catalytic properties. *Nano Res.* **2015**, *8*, 82–96.
73. Yuan, Y.; Yan, N.; Dyson, P.J. Advances in the Rational Design of Rhodium Nanoparticle Catalysts: Control via Manipulation of the Nanoparticle Core and Stabilizer. *ACS Catal.* **2012**, *2*, 1057–1069.
74. Chambers, M.B.; Wang, X.; Elgrishi, N.; Hendon, C.H.; Walsh, A.; Bonnefoy, J.; Canivet, J.; Quadrelli, E.A.; Farrusseng, D.; Mellot-Draznieks, C.; et al. Photocatalytic Carbon Dioxide Reduction with Rhodium-based Catalysts in Solution and Heterogenized within Metal-Organic Frameworks. *ChemSusChem* **2015**, *8*, 603–608.
75. Zhang, X.; Li, X.; Zhang, D.; Su, N.Q.; Yang, W.; Everitt, H.O.; Liu, J. Product selectivity in plasmonic photocatalysis for carbon dioxide hydrogenation. *Nat. Commun.* **2017**, *8*, 14542.
76. Chen, Y.; Chen, Q.S.; Peng, S.Y.; Wang, Z.Q.; Lu, G.; Guo, G.C. Manipulating the concavity of rhodium nanocubes enclosed by high-index facets via site-selective etching. *Chem. Commun. (Camb. Engl.)* **2014**, *50*, 1662–1664.
77. Gutiérrez, Y.; Ortiz, D.; Saiz, J.; González, F.; Everitt, H.; Moreno, F. The UV Plasmonic Behavior of Distorted Rhodium Nanocubes. *Nanomaterials* **2017**, *7*, 425.
78. Ahmadivand, A.; Sinha, R.; Kaya, S.; Pala, N. Rhodium Plasmonics for Deep-Ultraviolet Bio-Chemical Sensing. *Plasmonics* **2016**, *11*, 839–849.
79. Al-Kuhaili, M.F.; Durrani, S.M.A.; Khawaja, E.E. Optical properties of gallium oxide films deposited by electron-beam evaporation. *Appl. Phys. Lett.* **2003**, *83*, 4533.
80. Alcaraz de la Osa, R.; Sanz, J.M.; Barreda, A.I.; Saiz, J.M.; González, F.; Everitt, H.O.; Moreno, F. Rhodium Tripod Stars for UV Plasmonics. *J. Phys. Chem. C* **2015**, *119*, 12572–12580.
81. Nie, S. Probing Single Molecules and Single Nanoparticles by Surface-Enhanced Raman Scattering. *Science* **1997**, *275*, 1102–1106.
82. Taminiau, T.H.; Stefani, F.D.; Segerink, F.B.; van Hulst, N.F. Optical antennas direct single-molecule emission. *Nat. Photonics* **2008**, *2*, 234–237.
83. Savage, K.J.; Hawkeye, M.M.; Esteban, R.; Borisov, A.G.; Aizpurua, J.; Baumberg, J.J. Revealing the quantum regime in tunnelling plasmonics. *Nature* **2012**, *491*, 574–577.
84. Esteban, R.; Borisov, A.G.; Nordlander, P.; Aizpurua, J. Bridging quantum and classical plasmonics with a quantum-corrected model. *Nat. Commun.* **2012**, *3*, 825.

85. Rechberger, W.; Hohenau, A.; Leitner, A.; Krenn, J.R.; Lamprecht, B.; Aussenegg, F.R. Optical properties of two interacting gold nanoparticles. *Opt. Commun.* **2003**, *220*, 137–141.
86. Liao, P.F. Lightning rod effect in surface enhanced Raman scattering. *J. Chem. Phys.* **1982**, *76*, 751.